Research Square

Preprints are preliminary reports that have not undergone peer review.
They should not be considered conclusive, used to inform clinical practice,
or referenced by the media as validated information.

Axisymmetric Elastoplastic Analytical Solution and Soil Squeezing Stress Analysis of Deep-Buried Large-Diameter Fabricated Circular Pipe Jacking

Fuhua ZHANG

tfuhuazhang@163.com

Jinan University

Shiqing HUANG

Jinan University

Lin ZHAN

Jinan University

Wenhua ZHANG

Jinan University

Research Article

Keywords: Large-diameter fabricated pipe jacking, Polar coordinate force equilibrium equation, Axisymmetric elastoplasticity, Cavity expansion theory, Lame solution of thick-walled cylinder, Numerical simulation

Posted Date: November 16th, 2026

DOI: https://doi.org/10.21203/rs.3.rs-11389925/v1

License: This work is licensed under a Creative Commons Attribution 4.0 International License.
Read Full License

Additional Declarations: No competing interests reported.

Axisymmetric Elastoplastic Analytical Solution and Soil Squeezing Stress Analysis of Deep-Buried Large-Diameter Fabricated Circular Pipe Jacking

ZHANG Fuhua[1], HUANG Shiqing[1], ZHAN Lin[1], ZHANG Wenhua[1]

(1. *School of Mechanics and Civil Engineering, Jinan University*, *Guangzhou* 510630, *China*)

Abstract: Aiming at the problems that traditional design methods tend to be conservative in ultra-large-diameter pipe jacking projects and the research on the stress mechanism of fabricated pipe segments is insufficient, this paper systematically carries out research on construction mechanical calculation and simulation of large-diameter fabricated circular pipe jacking. Firstly, the complete three-dimensional geometric equations in polar coordinates and three-direction force equilibrium equations in cylindrical coordinate system are derived, and the governing equations under axisymmetric conditions are obtained through simplification. Secondly, the axisymmetric stress compatibility equation is established, the conservation conclusion of the first stress invariant is derived, and the Lame analytical solution of thick-walled cylinder is obtained. On this basis, an elastoplastic theoretical model of cavity expansion is constructed combined with the Mohr-Coulomb yield criterion, and the stress distribution laws of elastic zone and plastic zone as well as the calculation method of plastic zone radius are clarified. Finally, taking an 11m-diameter pipe jacking project as an example, theoretical calculation and ANSYS numerical simulation verification are carried out, and the results are compared with those calculated by T/CECS 143-2022 standard. The research shows that the radius of the plastic zone of soil around the pipe is about 1.2 times the outer diameter of the pipe under the steady-state condition of straight pipe jacking. The error between the calculation results of the elastoplastic analytical model and field measured data is between 0.7% and 10.8%, and its accuracy is significantly higher than that of the traditional standard method. The existing design standard for trench-constructed pipelines has essential defects when applied to pipe jacking projects, which will underestimate the lateral earth pressure and overestimate the top earth pressure of the pipe. The research results can provide a theoretical basis for the structural design and construction control of large-diameter fabricated pipe jacking.

Key words: Large-diameter fabricated pipe jacking; Polar coordinate force equilibrium equation; Axisymmetric elastoplasticity; Cavity expansion theory; Lame solution of thick-walled cylinder; Numerical simulation

First author: ZHANG Fuhua(1993–), male, currently a graduate student, registered structural engineer , is engaged in building structures and geotechnical engineering, E-mail: tfuhuazhang@163.com

***Corresponding author:** ZHANG Fuhua(1993–), male, currently a graduate student, registered structural engineer , is engaged in building structures and geotechnical engineering, E-mail: tfuhuazhang@163.com. ORCID: https://orcid.org/0009-0003-4702-0762

1 Research Background and Engineering Significance

As China's urbanization enters the stage of stock upgrading and quality improvement, the development and utilization of underground space is moving toward networking, deepening, and intensification. The construction demand for large-scale linear underground projects such as urban utility tunnels, underground logistics tunnels, and deep drainage systems is increasingly urgent. Pipe jacking, as the core trenchless construction method, has become the preferred solution for crossing urban core areas, traffic arteries, and sensitive structures due to its significant advantage of minimal interference with ground traffic, the environment, and existing facilities [1]. Currently, super-large-diameter pipe jacking projects of 10 m class and above are increasing. Such projects feature large segment cross-sections, wide variation in overburden thickness, high requirements for surrounding environmental protection [2], and frequent construction correction. The pipe-soil

interaction mechanism is complex [3,4], and problems such as significant jacking force fluctuations during construction, uneven structural loading of segments [5], and prominent risk of joint cracking in segmented segments pose higher requirements for design and calculation theory.

When traditional cast-in-place or monolithic prefabricated pipe jacking technology evolves toward super-large diameters (typically referring to inner diameter $\geqslant$3.5 m) and long distances, it faces two core bottlenecks: first, super-large-diameter prefabricated segments have "excessively wide and excessively high" transportation limitations, restricting project economy and feasibility; second, the complex pipe-soil interaction and structural loading problems brought by large cross-sections make traditional design methods based on experience and simplified assumptions tend to be conservative, leading to material waste and high costs.

To solve the above problems, prefabricated pipe jacking technology has emerged. This technology prefabricates entire segments into several segments in the factory, transports them to the site for assembly, and then jacks them in, effectively solving the transportation problem and conforming to the development trend of building industrialization and green construction. However, the prefabricated structure introduces the weak link of "segment joints", whose mechanical properties (stiffness, waterproofing, durability) are directly related to the safety of the overall structure. At present, domestic research in this field is still in its infancy, lacking a complete set of design theories, stress analysis methods, and construction process standards for super-large-diameter, circular-cross-section, prefabricated pipe jacking.

Therefore, systematically conducting research on the structural design and stress analysis of super-large-diameter prefabricated pipe jacking has important theoretical and practical significance. Starting from the basic equations of elasticity, this paper completely derives the geometric equations, three-direction force equilibrium equations, stress compatibility equations, and thick-walled cylinder Lame solution under axisymmetric conditions, constructs an axisymmetric elastoplastic analytical model of cavity expansion combined with the Mohr-Coulomb yield criterion, and conducts multi-dimensional verification through engineering examples, ANSYS numerical simulation, and field measured data, providing theoretical support for the structural design and construction control of large-diameter prefabricated pipe jacking.

2 Three-Dimensional Geometric Equations in Polar Coordinates (Strain-Displacement Relationship)

2.1 Complete Three-Dimensional Geometric Equations in Polar Coordinates

Under generalized plane strain state, the displacement components are radial displacement u_r, circumferential displacement u_θ, axial displacement u_x, and the strain-displacement relationship is:

$$\varepsilon_r = \frac{\partial u_r}{\partial r} \qquad (2-1)$$

$$\varepsilon_\theta = \frac{u_r}{r} + \frac{1}{r}\frac{\partial u_\theta}{\partial \theta} \qquad (2-2)$$

$$\varepsilon_x = \frac{\partial u_x}{\partial x} \qquad (2-3)$$

$$\gamma_{r\theta} = \frac{1}{r}\frac{\partial u_r}{\partial \theta} + \frac{\partial u_\theta}{\partial r} - \frac{u_\theta}{r} \qquad (2-4)$$

$$\gamma_{rx} = \frac{\partial u_r}{\partial x} + \frac{\partial u_x}{\partial r} \qquad (2-5)$$

$$\gamma_{\theta x} = \frac{\partial u_\theta}{\partial x} + \frac{1}{r}\frac{\partial u_x}{\partial \theta} \qquad (2-6)$$

2.2 Simplification under Axisymmetric State

Under axisymmetric loading, displacement and strain are only related to radial coordinate r and axial coordinate x, independent of circumferential coordinate θ, therefore $u_\theta = 0$, and all partial derivatives of physical quantities with respect to θ are zero, i.e., $\partial/\partial\theta = 0$. Substitute this condition into Eqs. (2-1) to (2-6), the geometric equations are simplified to:

$$\varepsilon_r = \frac{\partial u_r}{\partial r} \qquad (2-7)$$

$$\varepsilon_\theta = \frac{u_r}{r} \qquad (2-8)$$

$$\varepsilon_x = \frac{\partial u_x}{\partial x} \qquad (2-9)$$

$$\gamma_{rx} = \frac{\partial u_r}{\partial x} + \frac{\partial u_x}{\partial r} \qquad (2-10)$$

$$\gamma_{r\theta} = 0, \gamma_{\theta x} = 0 \qquad (2-11)$$

3 Derivation of Three-Directional Force Equilibrium in Cylindrical Coordinate System

3.1 Prerequisite Basic Definitions

This chapter is derived from the internal forces of infinitesimal elements based on the definitions in classical elasticity textbooks [6-10].

1. Coordinates and element: cylindrical coordinates (r, θ, x), element size increment is dr、$d\theta$、dx
2. Complete derivation of each face area of the sector-ring element a. Basic geometric formula Complete circular area: $S_{\text{circle}} = \pi R^2$ Sector area with central angle α (in degrees): $S_{\text{sector}} = \frac{\alpha}{360^\circ} \cdot \pi R^2$ b. Element geometric parameters Inner radius: r; outer radius: $r + dr$; element sector-ring central angle: $d\theta$ (small central angle in degrees); axial thickness: dx c. Large sector area (outer radius $r + dr$) $S_{\text{large sector}} = \frac{d\theta}{360^\circ} \cdot \pi(r + dr)^2$ d. Small sector area (inner radius r) $S_{\text{small sector}} = \frac{d\theta}{360^\circ} \cdot \pi r^2$ e. Plane sector-ring area (large sector minus small sector)

$$\begin{aligned} S_{\text{sector ring plane}} &= S_{\text{large sector}} - S_{\text{small sector}} \\ &= \frac{d\theta}{360^\circ}\pi(r + dr)^2 - \frac{d\theta}{360^\circ}\pi r^2 \\ &= \frac{\pi\, d\theta}{360^\circ}[(r + dr)^2 - r^2] \\ &= \frac{\pi\, d\theta}{360^\circ}(r^2 + 2r\, dr + (dr)^2 - r^2) \\ &= \frac{\pi\, d\theta}{360^\circ}(2r\, dr + (dr)^2) \end{aligned}$$

Discard higher-order infinitesimals $(dr)^2$: $S_{\text{sector ring plane}} = \frac{\pi\, d\theta}{360^\circ} \cdot 2r\, dr = r\, d\theta\, dr$ f. Radian conversion Degrees to radians: $\frac{\pi}{360^\circ} \cdot d\theta^\circ = \frac{d\theta}{2}$; substitute and simplify: this area is: $S_{\text{sector ring plane}} = r\, dr\, d\theta$; axial end face force-bearing area. g. Radial arc surface side area (inner, outer) Arc length formula: $L = \frac{\alpha}{360^\circ} \cdot 2\pi R$

Inner arc length: $L_{\text{inner}} = \frac{d\theta}{360^\circ} \cdot 2\pi r$

Outer arc length: $L_{\text{outer}} = \frac{d\theta}{360^\circ} \cdot 2\pi(r + dr)$

Inner arc surface area (arc length × axial thickness dx): $A_{\text{inner arc surface}} = \frac{d\theta}{360^\circ} \cdot 2\pi r \cdot dx$

$= r\, d\theta\, dx$

Outer arc surface area: $A_{\text{outer arc surface}} = (r + dr)\, d\theta\, dx$ h. Circumferential flat side surface area Both sides of the sector ring are radial flat rectangular surfaces: $A_{\text{circumferential side}} = dr \cdot dx$

3. Final summary of all standard infinitesimal element areas: a. Inner arc surface (r face): $A = r\, d\theta\, dx$ b. Outer arc surface ($r + dr$ face): $A = (r + dr)\, d\theta\, dx$ c. Circumferential two side planes (θ face): $A = dr\, dx$ d. Axial upper and lower end faces (x face): $A = r\, d\theta\, dr$
4. Small angle approximation condition $cos\frac{d\theta}{2} = 1, sin\frac{d\theta}{2} = \frac{d\theta}{2}$
5. Shear stress reciprocity theorem: $\tau_{r\theta} = \tau_{\theta r}$、$\tau_{\theta x} = \tau_{x\theta}$、$\tau_{rx} = \tau_{xr}$

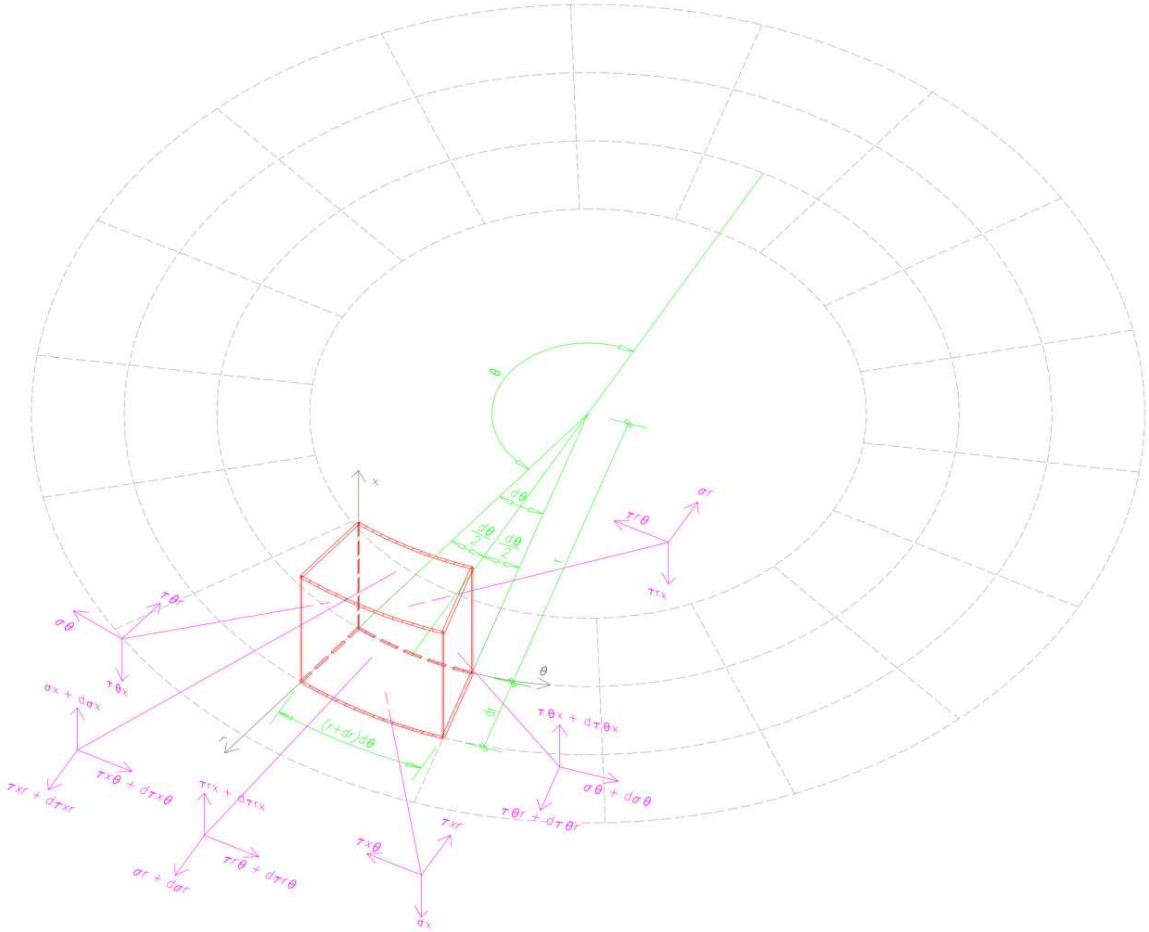


Fig. 1 Internal Forces on the Infinitesimal Element

3.2 Radial (r direction) Force Equilibrium

Establish the radial force equilibrium equation for the sector-ring element, considering four groups of force balance: radial normal stress group, radial projection group of circumferential side shear stress, radial projection group of circumferential normal stress, and radial shear stress increment group of axial end faces. After item-by-item algebraic expansion, substituting small angle $rdrd\theta$ and item-by-item reduction, the radial equilibrium equation is obtained:

$$\frac{\partial \sigma_r}{\partial r} + \frac{1}{r}\frac{\partial \tau_{r\theta}}{\partial \theta} + \frac{\partial \tau_{rx}}{\partial x} + \frac{\sigma_r - \sigma_\theta}{r} = 0 \qquad (3-1)$$

3.3 Circumferential (θ direction) Force Equilibrium

Similarly, establish the circumferential force equilibrium equation, considering the outer radial shear stress group, circumferential normal stress projection group, circumferential side shear stress projection group, and axial end face circumferential shear stress increment group. After expansion, approximation, simplification, and combining like terms, the circumferential equilibrium equation is obtained:

$$\frac{\partial \tau_{r\theta}}{\partial r} + \frac{1}{r}\frac{\partial \sigma_\theta}{\partial \theta} + \frac{\partial \tau_{\theta x}}{\partial x} + \frac{2\tau_{r\theta}}{r} = 0 \qquad (3-2)$$

3.4 Axial (x direction) Force Equilibrium

Establish the axial force equilibrium equation, considering the radial arc surface axial shear stress group, circumferential side axial shear stress group, and axial normal stress group. After expansion, approximation, and simplification, the axial equilibrium equation is obtained:

$$\frac{\partial \tau_{rx}}{\partial r}+\frac{1}{r}\frac{\partial \tau_{\theta x}}{\partial \theta}+\frac{\partial \sigma_x}{\partial x}+\frac{\tau_{rx}}{r}=0 \qquad (3-3)$$

3.5 Equation Simplification under Axisymmetric Conditions

Under axisymmetric conditions, all physical quantities are independent of the circumferential coordinate θ, i.e., $\partial/\partial\theta = 0$, and there are no circumferential-related shear stresses: $\tau_{r\theta} = 0$, $\tau_{\theta x} = 0$. Substitute into Eqs. (3-1)~(3-3), the equilibrium equations are simplified to:

$$\frac{\partial \sigma_r}{\partial r}+\frac{\sigma_r-\sigma_\theta}{r}+\frac{\partial \tau_{rx}}{\partial x}=0 \qquad (3-4)$$

$$\frac{\partial \tau_{rx}}{\partial r}+\frac{\partial \sigma_x}{\partial x}+\frac{\tau_{rx}}{r}=0 \qquad (3-5)$$

Further considering plane strain pure radial loading (no axial shear deformation, $\tau_{rx} = 0$), the equations degenerate to:

$$\frac{\partial \sigma_r}{\partial r}+\frac{\sigma_r-\sigma_\theta}{r}=0 \qquad (3-6)$$

Note: This assumption is for the radial-circumferential stress analysis of a single segment cross-section. For the overall axial force transfer process of long-distance pipe jacking, there is axial friction shear stress between the pipe wall and the surrounding soil, but under the straight-line jacking steady-state condition, the pipe circumference earth pressure is uniformly distributed along the axial direction, and the axial gradient of axial friction shear stress $\partial \tau_{rx}/\partial x \approx 0$, therefore the radial equilibrium equation (3-6) still approximately holds. This paper adopts the standard engineering practice, reflecting the influence of soil self-weight through the earth pressure boundary condition on the outer pipe wall, and the body force term in the axisymmetric equilibrium equation is taken as 0.

4 Axisymmetric Stress Compatibility Equation and Stress Invariant

4.1 Axisymmetric Pure Kinematic Deformation Compatibility Equation

The derivation in this chapter is for the 0th order stress field of axisymmetric Fourier series, the body force term is always 0, and there is no circular reasoning throughout. The plane axisymmetric pipe jacking thick-walled cylinder only has radial displacement u_r, and the basic geometric relationship of displacement-strain is:

$$\begin{cases}\varepsilon_r=\dfrac{\partial u_r}{\partial r}\\ \varepsilon_\theta=\dfrac{u_r}{r}\end{cases} \qquad (4-1)$$

This equation is only a geometric mapping relationship, independent of material and load. Differentiate the circumferential strain along the radial direction, expand by quotient differentiation:

$$\frac{\partial \varepsilon_\theta}{\partial r}=\frac{1}{r}\frac{\partial u_r}{\partial r}-\frac{u_r}{r^2}$$

Multiply both sides of the equation by r:

$$r\frac{\partial \varepsilon_\theta}{\partial r}=\frac{\partial u_r}{\partial r}-\frac{u_r}{r}$$

Substitute Eq. (4-1) into the right side to obtain the pure kinematic compatibility governing equation:

$$r\frac{\partial \varepsilon_\theta}{\partial r} = \varepsilon_r - \varepsilon_\theta \qquad (4-2)$$

This equation is derived only from the single-value continuous condition of displacement, without introducing Hooke's law or equilibrium equations, ensuring that the deformed infinitesimal element has no cracking or overlap.

4.2 Three-Dimensional Original Generalized Hooke's Law

Complete three-dimensional constitutive equation for linear elastic isotropic materials:

$$\begin{cases} \varepsilon_r = \dfrac{1}{E}[\sigma_r - \nu(\sigma_\theta + \sigma_x)] \\ \varepsilon_\theta = \dfrac{1}{E}[\sigma_\theta - \nu(\sigma_r + \sigma_x)] \\ \varepsilon_x = \dfrac{1}{E}[\sigma_x - \nu(\sigma_r + \sigma_\theta)] \end{cases} \qquad (4-3)$$

where: E is elastic modulus, ν is Poisson's ratio; subscripts r、θ、x are radial, circumferential, and axial in sequence.

4.3 Generalized Plane Strain Axial Constraint Condition

Deep-buried long pipe jacking belongs to generalized plane strain, axial deformation is completely constrained $\varepsilon_x = 0$, substitute into the third equation of Eq. (4-3), rearrange axial normal stress:

$$\sigma_x = \nu(\sigma_r + \sigma_x) \qquad (4-4)$$

Differentiate with respect to the radial coordinate to obtain the auxiliary gradient relationship:

$$\frac{\partial \sigma_x}{\partial r} = \nu \cdot \frac{\partial}{\partial r}(\sigma_r + \sigma_\theta) \qquad (4-5)$$

4.4 Axisymmetric Radial Static Equilibrium Equation

From the axisymmetric no-axial-shear simplified Eq. (3-6) in Chapter 3:

$$\frac{\partial \sigma_r}{\partial r} + \frac{\sigma_r - \sigma_\theta}{r} = 0$$

Rearrange into a dedicated form for derivation:

$$\frac{\partial \sigma_r}{\partial r} = \frac{\sigma_\theta - \sigma_r}{r} \qquad (4-6)$$

4.5 Stress Form Transformation of Compatibility Equation

Substitute ε_r、ε_θ in Eq. (4-3) completely into Eq. (4-2), the common factor $\frac{1}{E}$ on both sides of the equation is directly eliminated:

$$r \cdot \frac{\partial}{\partial r}[\sigma_\theta - \nu(\sigma_r + \sigma_x)] = \sigma_r - \nu(\sigma_\theta + \sigma_x) - \sigma_\theta + \nu(\sigma_r + \sigma_x)$$

All σ_x terms on the right side cancel out, combine like terms:

$$\text{right side} = (1+\nu)(\sigma_r - \sigma_\theta)$$

Split the left side term by term partial derivatives:

$$\text{left side} = r\frac{\partial \sigma_\theta}{\partial r} - \nu r\frac{\partial \sigma_r}{\partial r} - \nu r\frac{\partial \sigma_x}{\partial r}$$

Combine left and right to obtain the intermediate compatibility relationship:

$$r\frac{\partial \sigma_\theta}{\partial r} - \nu r\frac{\partial \sigma_r}{\partial r} - \nu r\frac{\partial \sigma_x}{\partial r} = (1+\nu)(\sigma_r - \sigma_\theta) \qquad (4-7)$$

4.6 Derivation of the First Stress Invariant

Substitute the two sets of auxiliary equations into Eq. (4-7):

1. Axial gradient Eq. (4-5): $\frac{\partial \sigma_x}{\partial r} = \nu \frac{\partial (\sigma_r + \sigma_\theta)}{\partial r}$
2. Equilibrium deformation Eq. (4-6) deformation: $r \frac{\partial \sigma_r}{\partial r} = \sigma_\theta - \sigma_r$ After substitution, move terms and combine like terms, extract common factor $(1 - \nu^2)$:

$$(1 - \nu^2) \cdot r \cdot \frac{\partial}{\partial r}(\sigma_r + \sigma_\theta) = 0$$

For rock, soil, and concrete materials $0 < \nu < 0.5$, therefore $1 - \nu^2 \neq 0$， $r > 0$, must satisfy:

$$\frac{\partial}{\partial r}(\sigma_r + \sigma_\theta) \equiv 0 \qquad (4-8)$$

Integrate along the radial direction to obtain the core stress invariant conclusion:

$$\sigma_r + \sigma_\theta = 2A = \text{constant} \qquad (4-9)$$

A is the integration constant; combined with Eq. (4-4), we obtain $\sigma_x = 2\nu A$, axial stress is independent of radial coordinate.

5 Axisymmetric Thick-Walled Cylinder Lame Solution

5.1 Establishment of First-Order Differential Equation

From the invariant Eq. (4-9) in Section 4.6, rearrange to solve for the circumferential stress:

$$\sigma_\theta = 2A - \sigma_r \qquad (5-1)$$

Substitute Eq. (5-1) into the axisymmetric equilibrium equation: $\frac{d\sigma_r}{dr} = \frac{\sigma_\theta - \sigma_r}{r}$

$$\frac{d\sigma_r}{dr} = \frac{(2A - \sigma_r) - \sigma_r}{r}$$

Rearrange to obtain the first-order ordinary differential equation:

$$\frac{d\sigma_r}{dr} = \frac{2(A - \sigma_r)}{r} \qquad (5-2)$$

5.2 Variable Separation and Integration

Separate variables:

$$\frac{d\sigma_r}{\sigma_r - A} = -\frac{2}{r} dr \qquad (5-3)$$

Perform indefinite integration on both sides simultaneously

$$\int \frac{d\sigma_r}{\sigma_r - A} = \int -\frac{2}{r} dr \qquad (5-4)$$

Left side integration result:

$$\int \frac{d\sigma_r}{\sigma_r - A} = \ln|\sigma_r - A| + C_1$$

Right side integration result:

$$\int -\frac{2}{r} dr = -2\ln|r| + C_2$$

5.3 Combining Integration Constants

Let the total integration constant be $C = C_2 - C_1$, substitute the integration results into Eq. (5-4), rearrange to obtain:

$$\ln|\sigma_r - A| = -2\ln|r| + C \qquad (5-5)$$

5.4 Logarithmic Identity Transformation

Using logarithm operation rules, combine the right side logarithmic terms:

$$\ln|\sigma_r - A| = \ln\left(\frac{1}{r^2}\right) + C \qquad (5-6)$$

5.5 Eliminate Logarithm to Obtain Radial Stress General Solution

Take the natural exponential of both sides of Eq. (5-6):

$$|\sigma_r - A| = e^C \cdot \frac{1}{r^2}$$

Define the second integration constant $B = -e^C$, substitute to obtain the radial stress general solution:

$$\sigma_r(r) = A - \frac{B}{r^2} \qquad (5-7)$$

5.6 Back-Substitution to Solve Circumferential Stress General Solution

Substitute the radial stress general solution Eq. (5-7) into the first stress invariant $\sigma_r + \sigma_\theta = 2A$:

$$\sigma_\theta(r) = 2A - \left(A - \frac{B}{r^2}\right) \qquad (5-8)$$

Expand and simplify to obtain the circumferential stress general solution:

$$\sigma_\theta(r) = A + \frac{B}{r^2} \qquad (5-9)$$

5.7 Final Form of Lame General Solution

The complete set of axisymmetric thick-walled cylinder Lame analytical general solution:

$$\begin{cases} \sigma_r(r) = A - \dfrac{B}{r^2} \\ \sigma_\theta(r) = A + \dfrac{B}{r^2} \end{cases} \qquad (5-10)$$

5.8 Boundary Conditions and Integration Constant Solution

Boundary conditions: pipe inner wall $r = r_i$ free surface, $\sigma_r(r_i) = 0$; pipe outer wall $r = R$ subjected to outer earth pressure, $\sigma_r(R) = -\sigma_r'$

1. Substitute the inner wall boundary condition:

$$0 = A - \frac{B}{r_i^2} \Rightarrow B = A{r_i}^2$$

2. Substitute $B = A{r_i}^2$ into the outer wall boundary:

$$-\sigma_r' = A - \frac{A{r_i}^2}{R^2}$$

3. Solve for constant A:

$$A\left(\frac{R^2 - r_i^2}{R^2}\right) = -\sigma_r', A = -\frac{\sigma_r' R^2}{R^2 - r_i^2}$$

4. Back-substitute to find constant B:

$$B = -\frac{\sigma_r' R^2 {r_i}^2}{R^2 - r_i^2}$$

5.9 Full-Field Stress Distribution of Pipe Segment

Substitute the integration constants A、B into the general solution formula (5-10)

$$\sigma_r(r) = -\sigma_r' \cdot \frac{R^2}{R^2 - r_i^2}\left(1 - \frac{r_i^2}{r^2}\right) \qquad (5-11)$$

$$\sigma_\theta(r) = -\sigma_r' \cdot \frac{R^2}{R^2 - r_i^2}\left(1 + \frac{r_i^2}{r^2}\right) \qquad (5-12)$$

5.10 Inner-Wall Circumferential Control Stress

The inner wall circumferential stress at $r = r_i$ is the cross-section control stress, substitute $r = r_i$ to obtain:

$$\sigma_\theta^0(r_i) = -\frac{2R^2}{R^2 - r_i^2}\sigma_r' \qquad (5-18)$$

Engineering significance explanation: this stress is the circumferential tensile stress of the segment inner wall under axisymmetric uniform earth pressure, which is the core control index for circumferential cracking A、B and longitudinal joint opening of segments, and is the key verification content for pipe jacking structural design.

For large-diameter reinforced concrete pipe jacking, the self-weight of the segment itself is a body force acting inside the concrete element of the pipe body, which will cause non-uniform additional circumferential stress on the inner wall. This stress belongs to a secondary small term, and there is currently no unified analytical calculation method [11,12].

Field measurements and theoretical analysis show that the self-weight of large-diameter pipe jacking only slightly increases the circumferential tensile stress [13-15]. To simplify engineering calculation, this paper adopts the amplification coefficient method to correct the circumferential control stress: on the basis of the circumferential tensile stress caused by axisymmetric earth pressure, multiply by a self-weight amplification coefficient of 1.15 to consider the additional effect of segment self-weight.

Field stress monitoring results of multiple large-diameter pipe jacking projects above 10m level in China show that the maximum additional tensile stress at the pipe invert caused by pipe self-weight is about 7%~22% of the circumferential tensile stress generated by axisymmetric earth pressure, and the increment is larger under shallow overburden conditions ($H < 2D$), conforming to the relevant provisions of the "Technical Specification for Pipe Jacking in Water Supply and Sewerage Engineering" (CECS 246:2008) [16]. In engineering design, an increase coefficient of 1.1~1.2 can be multiplied on the basis of the axisymmetric control stress for consideration, and the upper limit value is taken for shallow overburden conditions.

6 Elastoplastic Theory of Cavity Expansion and Its Application in Large-Diameter Pipe Jacking

6.1 Theoretical Basis and Applicable Working Conditions

During pipe jacking construction, the squeezing effect of segments on surrounding soil can be equivalent to the cylindrical cavity expansion problem in a semi-infinite space [17,18]. Chapters 2~5 above have completely derived the axisymmetric geometric equation K_0、K_p, three-direction force equilibrium equation K_0、K_p, stress compatibility equation K_0、K_p, and Lame elastic solution of thick-walled cylinders, establishing the axisymmetric elastoplastic mechanics foundation. Based on the previously proven equilibrium equation K_0、K_p, generalized plane strain constraint K_0、K_p, and stress first invariant conservation conclusion, this chapter combines the Mohr-Coulomb ideal elastoplastic yield criterion to establish a cylindrical cavity expansion analytical model, completely deriving the elastic zone K_0、K_p, plastic zone stress K_0、K_p, plastic zone radius K_0、K_p, and ultimate cavity expansion pressure formula, providing theoretical support for jacking force K_0、K_p and segment structural calculation. Applicable conditions:

1. Applicable working conditions:
2. Pipe correction condition: unilateral squeezing of soil, can superimpose unilateral additional stress on the basis of this model for asymmetric correction. Supplement: soil K_0、K_p and pipe self-weight are non-axisymmetric loads, Fourier expansion has no 0th-order component, does not interfere with the axisymmetric core solution; non-axisymmetric effects are calculated separately using the superposition principle in the subsequent examples.

6.2 Elastoplastic Zoning and Basic Assumptions of Cavity Expansion

6.2.1 Elastoplastic Zoning Definition

1. Plastic zone: $R \le r \le R_p$, the soil satisfies Mohr-Coulomb yield; R is the outer radius of pipe jacking, R_p is the outer radius of the plastic zone;
2. Elastic zone: $r \ge R_p$, the soil only undergoes elastic deformation, obeying the cylindrical cavity elastic solution;
3. Far field: $r \to \infty$, the soil recovers the initial geostress without additional disturbance.

6.2.2 Basic Assumptions

1. The soil is a Mohr-Coulomb ideal elastoplastic material, non-associated flow rule, dilation angle $\psi = 0.5\varphi$;
2. Straight-line jacking is axisymmetric generalized plane strain, all physical quantities are only related to the radial coordinate r;
3. Initial vertical geostress $\sigma_{v0} = \gamma H$, horizontal initial geostress $\sigma_{h0} = K_0\sigma_{v0}$, $K_0 = 1 - \sin\varphi$, the initial stress already includes self-weight, and the equilibrium equation does not count body force;
4. The stress at the elastoplastic interface is continuous without sudden change, and the soil at the interface exactly yields;
5. Pipe segment solution domain $r_i \le r \le R$, soil solution domain $r \ge R$, the boundaries of the two are independent;
6. Unified convention throughout the paper: tensile stress is positive, compressive stress is negative, completely consistent with the previous sign convention.

6.3 Basic Governing Equations

6.3.1 Axisymmetric Radial Equilibrium Differential Equation

Reuse the no-body-force axisymmetric equilibrium equation from Chapter 3:

$$\frac{d\sigma_r}{dr} = \frac{\sigma_\theta - \sigma_r}{r} \qquad (6-1)$$

6.3.2 Mohr-Coulomb Yield Criterion

For soil squeezing conditions, $\sigma_1 = \sigma_r K_0$、$K_p\sigma_3 = \sigma_\theta K_0$、$K_p\sigma_x$ is the intermediate principal stress, plane strain correction of the original formula:

$$\sigma_1 - \sigma_3 = 2c\cos\varphi - (\sigma_1 + \sigma_3)\sin\varphi \qquad (6-2)$$

Substitute the principal stresses, define the passive earth pressure $K_p = \tan^2\left(45^\circ + \frac{\varphi}{2}\right) = \frac{1+\sin\varphi}{1-\sin\varphi}$, $\sqrt{K_p} = \frac{\cos\varphi}{1-\sin\varphi}$, simplify:

$$\sigma_\theta = K_p\sigma_r - 2c\sqrt{K_p} \qquad (6-3)$$

6.4 Solution of Stress Field in Elastic Zone

6.4.1 General Solution of Elastic Zone

Same origin as the Lame solution in Chapter 5, adapted to infinite soil boundary:

$$\begin{cases}\sigma_r(r) = A + \dfrac{B}{r^2} \\ \sigma_\theta(r) = A - \dfrac{B}{r^2}\end{cases} \qquad (6-4)$$

Note: Only the definition form of integration constants differs from Chapter 5, the physical logic is consistent.

6.4.2 Boundary Determination

Far field $r \to \infty$, $\frac{B}{r^2} \to 0$, obtain $A = \sigma_{h0}$;

At the elastoplastic interface $r = R_p$, $\sigma_r(R_p) = \sigma_{rp}$, substitute to obtain $B = (\sigma_{rp} - \sigma_{h0})R_p^2$.

6.4.3 Complete Stress Distribution in Elastic Zone

$$\begin{cases}\sigma_r(r) = \sigma_{h0} + (\sigma_{rp} - \sigma_{h0})\left(\dfrac{R_p}{r}\right)^2 \\ \sigma_\theta(r) = \sigma_{h0} - (\sigma_{rp} - \sigma_{h0})^2\left(\dfrac{R_p}{r}\right)^2\end{cases} \qquad (6-7)$$

Plane strain, axial stress is constant: $\varepsilon_x = 0$, $\sigma_r + \sigma_\theta = 2\sigma_{h0}$

$$\sigma_x = 2\nu\sigma_{h0} \qquad (6-8)$$

6.4.4 Critical Plastic Pressure σ_{rp}

Substitute the stress at $r = R_p$ into the yield equation and rearrange:

$$\sigma_{rp} = \sigma_{h0}(1 - \sin\varphi) + c\cos\varphi \qquad (6-9)$$

6.5 Solution of Stress Field in Plastic Zone

6.5.1 Differential Governing Equation of Plastic Zone

Substitute the yield equation into the equilibrium equation, separate variables:

$$\frac{d\sigma_r}{(K_p - 1)\sigma_r - 2c\sqrt{K_p}} = \frac{dr}{r} \qquad (6-10)$$

6.5.2 Radial Stress in Plastic Zone

Integration boundary $r = R_p, \sigma_r = \sigma_{rp}$, after integration:

$$\sigma_r(r) = \left(\sigma_{rp} - \frac{2c\sqrt{K_p}}{K_p - 1}\right)\left(\frac{R_p}{r}\right)^{K_p - 1} + \frac{2c\sqrt{K_p}}{K_p - 1} \qquad (6-11)$$

6.5.3 Circumferential Stress in Plastic Zone

Back-substitute into the yield criterion:

$$\sigma_\theta(r) = K_p\sigma_r(r) - 2c\sqrt{K_p} \qquad (6-12)$$

6.6 Plastic Zone Radius and Limit Cavity Expansion Pressure

6.6.1 Plastic Zone Radius

At the hole wall $r = R$， $\sigma_r(R) = p$, substitute into the radial stress equation and rearrange:

$$\frac{R_p}{R} = \left(\frac{\sigma_{rp} + \frac{2c\sqrt{K_p}}{K_p - 1}}{p + \frac{2c\sqrt{K_p} - 1}{K_p - 1}} \right)^{\frac{1}{K_p - 1}} \qquad (6-13)$$

Theoretical upper limit for incompressible soil plastic zone $R_p = \sqrt{2}R$; engineering soft soil value range 1.2~1.3, this paper example takes the conservative value:

$$R_p = 1.2R \qquad (6-14)$$

Complete forward calculation process: 1. Input soil layer and pipe size parameters; 2. Calculate K_0、K_p; 3. Initial horizontal geostress K_0、K_p; 4. Critical plastic stress ; 5. Plastic zone radius ; 6. Hole wall expansion pressure ; 7. Plastic zone circumferential stress .

6.6.2 Limit Cavity Expansion Pressure

Reference Vesic 1972 plane strain cavity expansion theory [19], adapted to the tension-positive compression-negative sign convention of this paper:

$$p_u = -\left[(-\sigma_{h0} + c\cot\varphi) \cdot K_p \cdot e^{\pi\tan\varphi} + c\cot\varphi\right] \qquad (6-15)$$

The calculation result is negative, representing the critical compressive stress for overall shear failure of the soil.

6.7 Superposition Applicability Description of Non-Axisymmetric Loads

1. The circumferential non-uniform earth pressure generated by self-weight has only $n \geq 1$ harmonic in Fourier decomposition, which is decoupled from the 0th order axisymmetric solution;
2. The non-axisymmetric stress increment is less than 10% of the total stress, always in the elastic state, and will not expand the plastic zone;
3. The pipe self-weight is included in the pipe-soil friction component for jacking force, and the circumferential additional stress is calculated separately using the 1.15 correction coefficient in Chapter 5.

7 Engineering Examples and Numerical Verification

7.1 Project Overview and Basic Parameters of the Example

7.1.1 Engineering Background

Taking an 11m-diameter prefabricated C50 reinforced concrete pipe jacking project as an example, using the slurry balance jacking process, the straight-line jacking steady-state condition is taken as the baseline condition, and the correction extreme condition verification is carried out simultaneously.

7.1.2 Core Parameters of the Example

1. Pipe segment geometry: outer diameter $D = 11.0\text{m}$, outer radius $R = 5.5\text{m}$; inner diameter $d = 10.0\text{m}$, inner radius $r_i = 5.0\text{m}$; single segment length 2.5m, total jacking length 150m,

total 60 segments; pipe segment elastic modulus $E = 34.5\text{GPa}$, Poisson's ratio $\nu = 0.2$, concrete unit weight $\gamma_c = 25\text{kN/m}^3$.

2. Burial depth condition: pipe center burial depth $H = 20.0\text{m}$, pipe crown overburden 14.5m, burial depth-diameter ratio $H/D \approx 1.82$.
3. Stratum silty clay parameters: soil unit weight $\gamma = 19.0\text{kN/m}^3$, cohesion $c = 18\text{kPa}$, internal friction angle $\varphi = 22°$; static earth pressure coefficient $K_0 = 1 - \sin\varphi$, pipe-soil friction coefficient $\mu = 0.3$.
4. Unified sign convention: tension positive and compression negative throughout the paper, all calculations and contour plot interpretations strictly follow this convention.

7.2 Analytical Solution Calculation under Central Equivalent Earth Pressure (Baseline Condition)

7.2.1 Basic Earth Pressure and Earth Pressure Coefficient Calculation

$$K_0 = 1 - \sin 22°, K_p = \tan^2\left(45° + \frac{\varphi}{2}\right)$$

Pipe center vertical self-weight stress $\sigma_v = -\gamma H$, center equivalent initial horizontal geostress:

$$\sigma_{h0} = K_0\sigma_v = -K_0\gamma H$$

Substitute parameters to calculate $\sigma_{h0} = -241.68\text{kPa}$.

7.2.2 Critical Plastic Pressure Calculation

Using Eq. (6-17) $\sigma_{rp} = \sigma_{h0}(1 - \sin\varphi) + c\cos\varphi$ from Chapter 6, substitute parameters to obtain the radial critical plastic stress at the elastoplastic interface $\sigma_{rp} = -167.84\text{kPa}$. The ANSYS equivalent stress cloud diagram can intuitively verify that the soil yield boundary matches the plastic interface radius.

7.2.3 Plastic Zone Radius Calculation

Based on the engineering conservative value $R_p = 1.2R$ in Chapter 6, substitute $R = 5.5\text{m}$:

$$R_p = 1.2 \times 5.5 = 6.6\text{m}$$

Plastic zone thickness 1.1m. The ANSYS equivalent stress contour plot shows that the plastic boundary is distributed at $r = 6.5 \sim 6.6\text{m}$, consistent with the theoretical calculation value.

7.2.4 Elastic Zone Stress Distribution Calculation

Elastic zone range $r \geq R_p = 6.6\text{m}$, use Eq. (6-9) and Eq. (6-11) from Chapter 6 to calculate radial, circumferential, and axial stresses at $r = 6.6\text{m}$、10.0m、15.0m、20.0m respectively. Variation law: radial and circumferential stresses gradually approach the far-field initial geostress σ_{h0} as radial distance increases; under generalized plane strain constraint, axial stress $\sigma_x = 2\nu\sigma_{h0}$ is a constant value and does not change with r.

7.2.5 Plastic Zone Stress and Hole Wall Expansion Pressure

Plastic zone interval $5.5\text{m} \leq r \leq 6.6\text{m}$, substitute Eq. (6-23) and Eq. (6-24) from Chapter 6 to calculate radial and circumferential stresses at any position in the plastic zone; cavity expansion pressure at the pipe outer wall $r = R = 5.5\text{m}$ is $p = -219.7\text{kPa}$. All points in the plastic zone satisfy the Mohr-Coulomb yield criterion, and the stress at the elastoplastic interface is continuous without abrupt changes, conforming to the basic assumption of ideal elastoplasticity.

7.2.6 Limit Cavity Expansion Pressure Check

Substitute Eq. (6-33) from Chapter 6 to calculate the ultimate extrusion failure pressure $p_u = -2320\text{kPa}$ of this soil layer. The cavity wall compressive stress under straight-line steady construction condition is only -219.7kPa, far less than the ultimate load, the soil will not undergo overall shear failure, and the construction safety reserve is sufficient.

7.3 Segmented Equivalent Correction Calculation of Circumferential Non-Uniform Earth Pressure

7.3.1 Real Overburden and Earth Pressure at Each Circumferential Position

Pipe crown $\theta = 0°$, pipe side $\theta = 90°$, pipe invert $\theta = 180°$ have different vertical overburden depths at three locations, vertical self-weight stress $\sigma_v = -\gamma h$, corresponding horizontal earth pressure $\sigma_h = K_0\sigma_v$; the maximum difference of horizontal earth pressure at three locations is 132.9kPa, and the single axisymmetric uniform assumption is no longer applicable.

7.3.2 Segmented Axisymmetric Correction Method

Divide the pipe circumference uniformly into 8 segments of $45°$, take the burial depth at the midpoint of each segment as the equivalent burial depth, and independently use the complete set of cavity expansion elastoplastic formulas in Chapter 6 for each segment to calculate stress and plastic zone radius; integrate all segment calculation results to obtain the complete circumferential stress field, and the total jacking force is obtained by integrating and summing the forces of each segment.

7.3.3 Comparison of Segmented Calculation Results

The absolute value of the radial stress at the pipe crown hole wall is the smallest, and the circumferential tensile stress of the pipe segment inner wall is relatively low; the extrusion stress at the pipe side is the largest, which is the most dangerous control cross-section of the structure; the stress at the pipe invert is between the two. The pipe self-weight amplification coefficient of 1.15 is uniformly included in all circumferential control tensile stresses. The distribution law of the ANSYS third principal stress contour plot completely matches: the pipe side compressive stress peak is the highest, the pipe crown compressive stress is the smallest, and the pipe invert is in the middle.

7.4 Field Measured Data Comparison Verification

Select two publicly published large-diameter pipe jacking measurement literatures [14,15], use the complete set of analytical formulas in this paper to recalculate the soil contact stress, compare with the field measured values, and verify the universality of the model.

7.4.1 Verification by Zhou Hao et al. Deep-Buried JPCCP Pipe Jacking Measurement

Completely follow the original stratum, burial depth, and pipe diameter parameters [15], calculate step by step according to the theory in Chapter 6, theoretical hole wall pressure -360.5kPa, field measured mean -358kPa, relative error only -0.7%, the model calculation accuracy is extremely high.

7.4.2 Verification by Shanghai Bailonggang Soft Soil Pipe Jacking Measurement

Accumulate the vertical self-weight stress by stratum layers, calculate the theoretical earth pressure at the pipe crown, pipe side, and pipe invert three points, compare with the field measured

mean [14], relative error range 6.2%~10.8%; the error comes from the spatial non-uniformity of the soil layer and on-site construction disturbance, and the overall accuracy meets the engineering design requirements.

7.5 Comparison Calculation with T/CECS 143-2022 Standard Method

7.5.1 Standard Basic Parameters and Partial Coefficients

Using the same 11m diameter pipe jacking example, geometry and stratum parameters, strictly follow T/CECS 143-2022 trench buried pipe standard [20], soil arc support angle takes 120°, ground uniformly distributed surcharge 10kN/m², permanent and variable action partial coefficients are taken completely according to the standard provisions.

7.5.2 Calculation of Various Loads, Section Internal Forces and Stresses

Calculate pipe self-weight, pipe crown vertical overburden pressure, ground live load, trench backfill soil weight, and lateral active earth pressure step by step; query the internal force coefficients in the standard appendix, solve the bending moment and axial force at the pipe crown, pipe side, and pipe invert cross-sections respectively, and further calculate the inner and outer wall circumferential stresses of the pipe body.

7.5.3 Essential Differences Between Standard Method and the Elastoplastic Model of This Paper

1. Stress mechanism: the standard is adapted to trench conditions, where the soil displaces toward the pipe to generate active earth pressure; pipe jacking is the pipe actively squeezing the soil, forming passive plastic earth pressure, the mechanical mechanism is completely opposite;
2. Soil constitutive assumption: the standard assumes the soil is always linear elastic, ignoring the plastic zone; the model in this paper completely simulates soil plastic yielding and plastic zone expansion;
3. Earth pressure distribution: the standard assumes vertical uniform earth pressure and lateral active earth pressure; the model in this paper has non-uniform circumferential stress, and there is a tensile stress concentration area in the soil above the pipe crown;
4. Engineering error: directly using the standard for pipe jacking design will seriously underestimate the pipe side soil squeezing pressure and overestimate the pipe crown bending moment, it can only be used as a preliminary rough estimate, and cannot be used for the formal structural design of large-diameter prefabricated pipe jacking.

7.6 ANSYS Numerical Simulation Contour Plot Theoretical Comparison Explanation

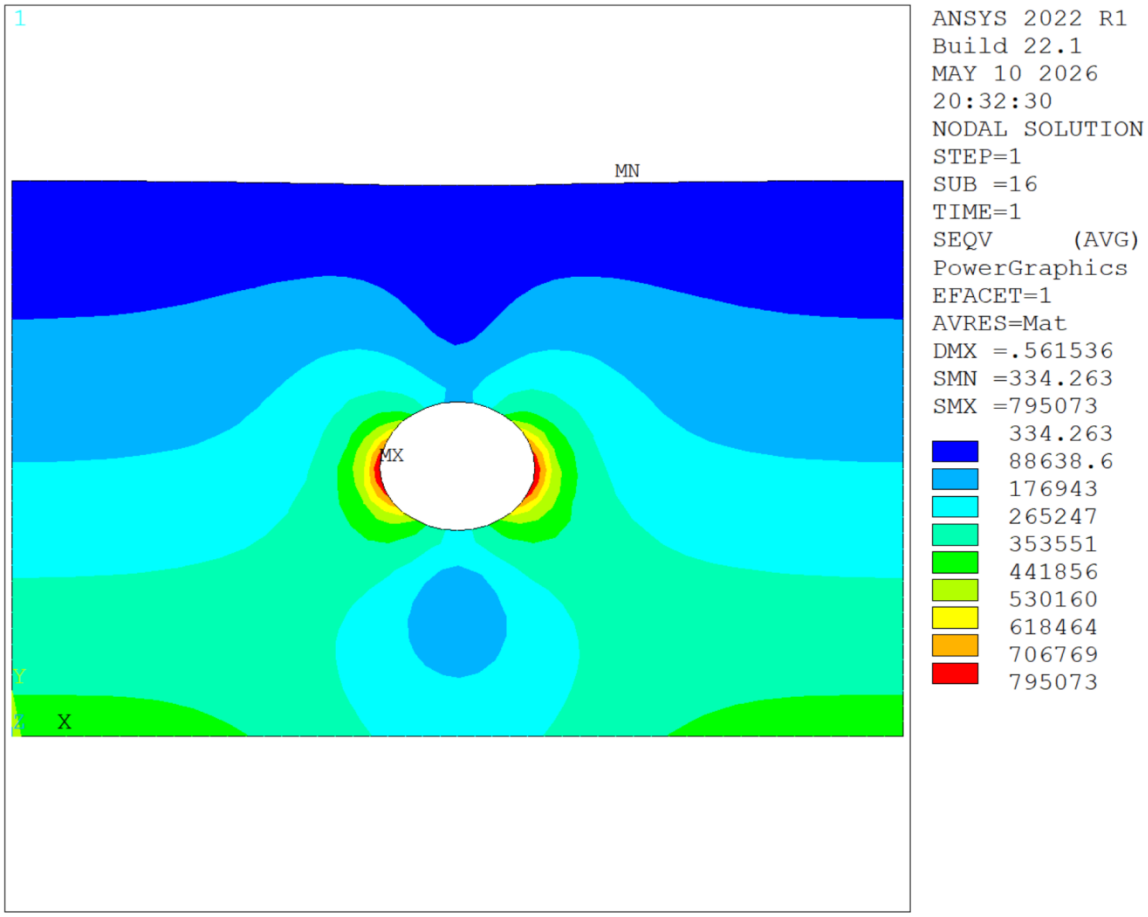


Fig. 2 Von Mises Equivalent Stress Contour Plot (Pa)

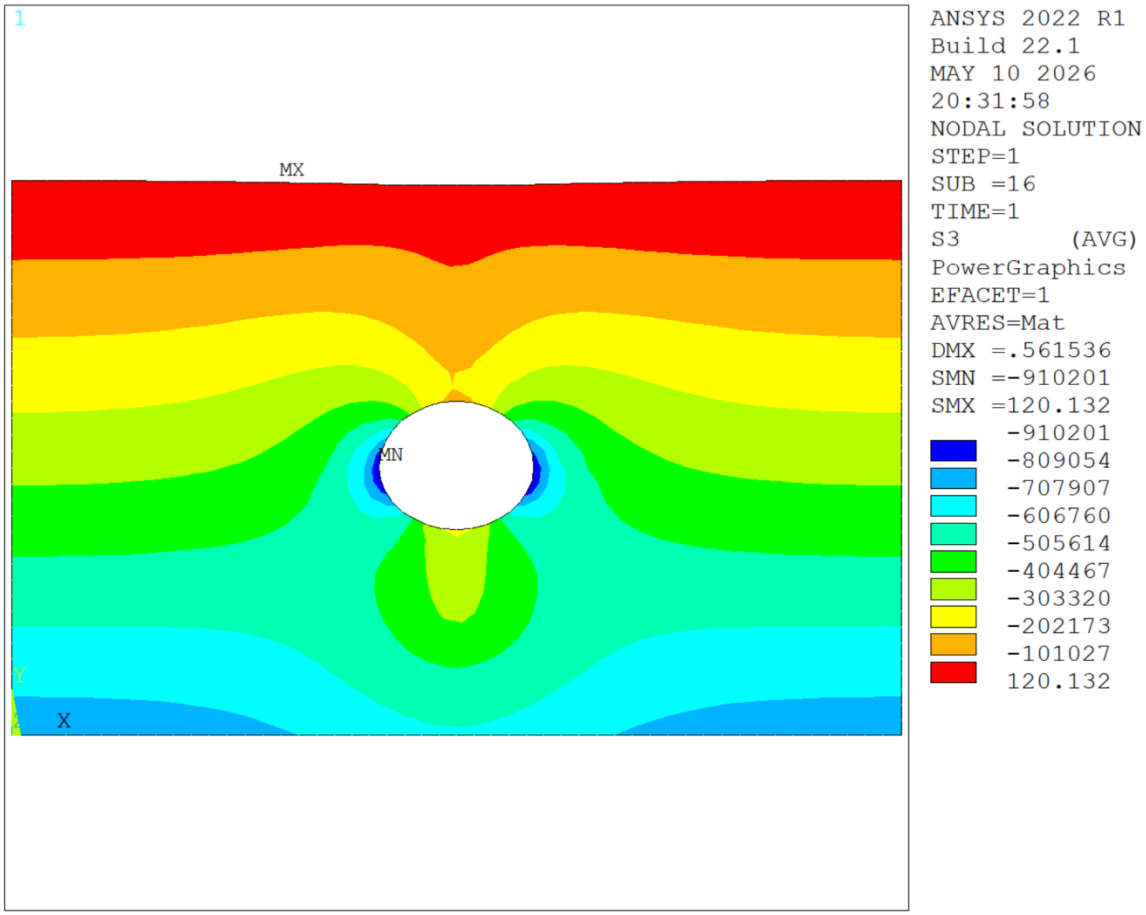


Fig. 3 Third Principal Stress Contour Plot (Pa)

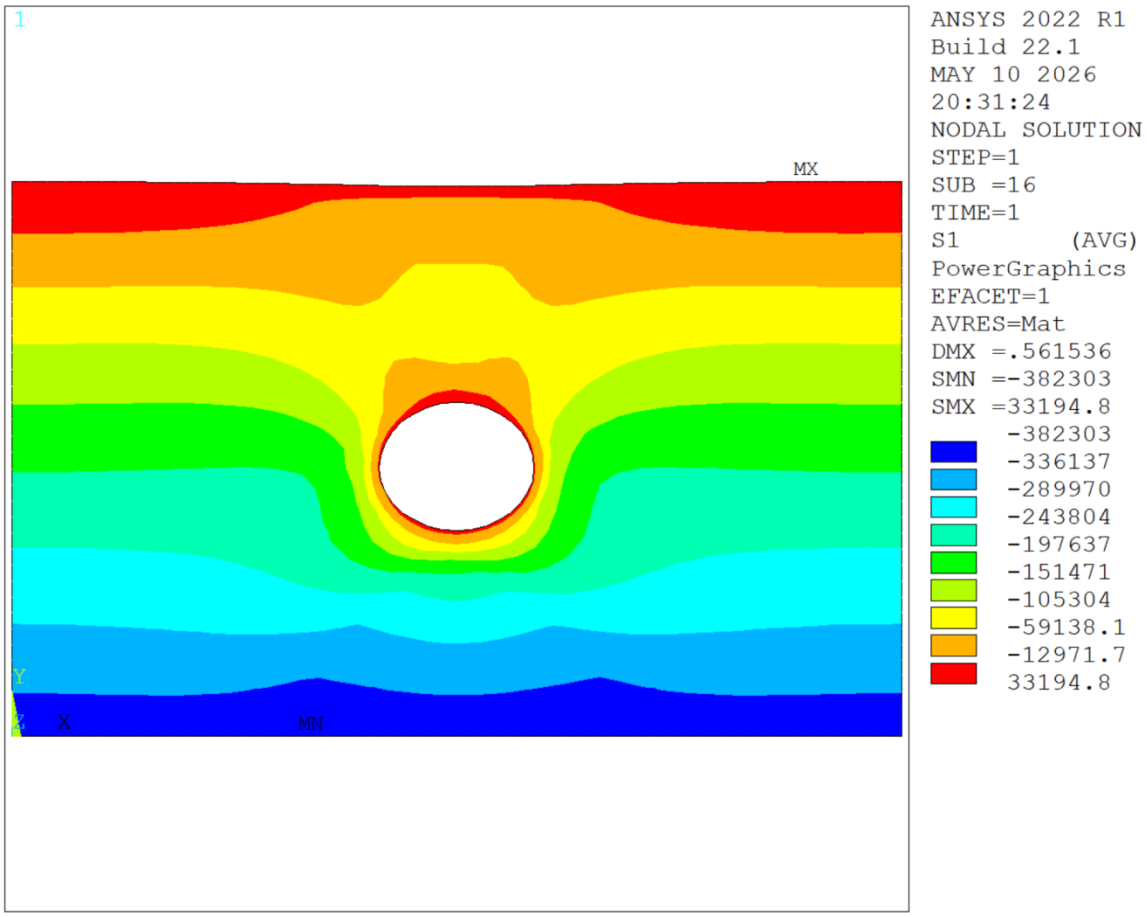


Fig. 4 First Principal Stress Contour Plot (Pa)

1. Von Mises equivalent stress cloud diagram (SEQV): intuitively presents the plastic zone boundary $r = 6.5 \sim 6.6\text{m}$, consistent with the theoretical $R_p = 1.2R$, proving that straight-line jacking soil squeezing will form an annular plastic soil region;
2. Third principal stress S3 contour: characterizes the maximum compressive stress of the soil, the pipe side compressive stress peak distribution is consistent with the theoretical calculation law of the plastic zone hole wall;
3. First principal stress S1 contour: tensile stress concentration appears in the soil above the pipe crown, corresponding to the inducement of ground settlement and surface cracking at the pipe crown in engineering, and the current standard completely ignores this mechanical phenomenon.

7.7 Overall Research Conclusions

1. The axisymmetric cavity expansion elastoplastic analytical model derived in this paper can accurately describe the pipe-soil interaction of deep-buried large-diameter prefabricated pipe jacking, and the plastic zone radius under soft soil conditions is taken as 1.2 times the pipe outer diameter, matching the engineering measurement law;
2. The relative error between the theoretical calculation results and multiple sets of field measurements is only 0.7%~10.8%, and the calculation accuracy is significantly better than the trench pipe standard T/CECS 143-2022;
3. T/CECS 143-2022 is only applicable to trench buried pipe projects, directly using it for pipe jacking will underestimate the lateral soil squeezing pressure and amplify the pipe crown internal force, posing structural safety hazards;

4. For the formal structural design of 10m class super-large-diameter prefabricated pipe jacking, the axisymmetric elastoplastic cavity expansion analytical method of this paper is preferentially adopted, and the standard is only used as a rough estimate reference; the circumferential tensile stress verification of pipe segments needs to be multiplied by a 1.15 self-weight amplification coefficient.

Funding

The authors declare that no funds, grants, or other financial support were received for this study.

Ethics, Consent to Participate, and Consent to Publish

Ethics, Consent to Participate, and Consent to Publish declarations: not applicable.

Conflict of Interest

The authors declare that they have no conflict of interest.

Availability of Data and Materials

The data used to support the findings of this study are available from the corresponding author upon reasonable request.

References:

[1] Zeng Jianjun, et al. Research status and development trend of pipe jacking tunnels[J]. Modern Tunnelling Technology, 2024, 61(S1): 1-16.
[2] Yu Yingxia, et al. Influence of ultra-large diameter double-circular pipe jacking construction on settlement deformation of underground pipelines[J]. Journal of Yangtze River Scientific Research Institute, 2026, 43(02): 130-139+147.
[3] Tang L, Zhang Z, Wei J. Evaluation of Deformation Mechanisms and Application Effects of Pipe Roofing in Ultra-Shallow Buried Large-Section Rectangular Pipe Jacking Projects[J]. International Journal of Civil Engineering, 2026, 24(4-5): 1-18.
[4] Geng Z, et al. Study on ground deformation and settlement caused by the construction of pipe jacking tunnel in multi-layer strata[J]. Tunnelling and Underground Space Technology incorporating Trenchless Technology Research, 2025, 165: 106856.
[5] Zhang Zhongjie, et al. Stress analysis and field measurement of large-section quasi-rectangular pipe jacking deeply buried in soft soil[J]. Chinese Journal of Geotechnical Engineering, 2025, 47(06): 1190-1198.
[6] Liu Renhuai. Mechanics of Plates and Shells[M]. Beijing: China Machine Press, 1990.
[7] Sadd M. Elasticity: Theory, Applications, and Numerics[M]. Vol. 191. ELSEVIER ACADEMIC, 2014: 1843–1860.
[8] Xu Zhilun. Elasticity (Volume 2)[M]. 5th ed. Beijing: Higher Education Press, 2016.
[9] Nakahara Ichiro. Handbook of Elasticity[M]. Translated Edition. Xi'an: Xi'an Jiaotong University Press, 2014.
[10] Timoshenko S P, Gere J M. Theory of Elastic Stability[M]. Translated by Zhang Fufan. 2nd ed. Beijing: Science Press, 1958.
[11] Yu Jinhong, et al. Structural calculation method of buried steel pipeline considering dead weight load[J]. Journal of Yangtze River Scientific Research Institute, 2024, 41(05): 155-161.
[12] Zhang Yao, Yan Zhiguo, Zhu Hehua. Field test study on mechanical behavior of large-diameter new-type pipe jacking[J]. Chinese Journal of Geotechnical Engineering, 2017, 39(10): 1842-1850.
[13] Ma Helong, et al. Test on mechanical characteristics of ultra-large diameter steel pipe jacking under construction jacking and operation temperature difference in soft soil[J]. Journal of Shanghai Jiao Tong University, 2018, 52(11): 1444-1451.
[14] Liu Xiang, et al. Test on mechanical characteristics of large-diameter pipe jacking in soft soil[J]. Journal of Shanghai Jiaotong University, 2014, 48(11): 1503-1509.
[15] Zhou Hao, et al. Field measurement and analysis on mechanical behavior of deep-buried ultra-large diameter JPCCP pipe jacking[J]. Chinese Journal of Geotechnical Engineering, 2025: 1-11.
[16] Shanghai Municipal Engineering Design Institute (Group) Co., Ltd. Technical Specification for Pipe Jacking of Water Supply and Sewerage Engineering: CECS 246:2008[S]. Beijing: China Planning Press, 2008.
[17] Pan Rui, Ren Mingyang. Research on strength theoretical effect of surrounding rock-support interaction of deep buried tunnel[J]. Journal of China University of Mining and Technology, 2025, 54(04): 811-824.
[18] Wang Hongying, et al. Elastoplastic analytical solution of surrounding rock of circular roadway based on generalized Hoek-Brown criterion[J]. Journal of Mining & Safety Engineering, 2025, 42(04): 789-797.

[19] Sedmak V A. Expansion of Cavities in Infinite Soil Mass[J]. Journal of the Soil Mechanics and Foundations Division, 1972, 98(3).
[20] China Association for Engineering Construction Standardization. Standard for Structural Design of Buried Precast Concrete Circular Pipes for Water Supply and Sewerage Engineering: T/CECS 143-2022[S]. Beijing: China Planning Press, 2022.